Atmos. Chem. Phys. Discuss., 11, 7235–7289, 2011
www.atmos-chem-phys-discuss.net/11/7235/2011/
doi:10.5194/acpd-11-7235-2011

Atmospheric Chemistry and Physics Discussions

Surface modification of mineral dust particles by sulphuric acid processing: implications for CCN and IN abilities

P. Reitz[1,2], C. Spindler[3], T. F. Mentel[3], L. Poulain[4], H. Wex[4], K. Mildenberger[4], D. Niedermeier[4], S. Hartmann[4], T. Clauss[4], F. Stratmann[4], R. C. Sullivan[5], P. J. DeMott[5], M. D. Petters[6], B. Sierau[7], and J. Schneider[1]

[1]Particle Chemistry Department, Max Planck Institute for Chemistry, Mainz, Germany
[2]Institute for Atmospheric Physics, Johannes Gutenberg University, Mainz, Germany
[3]Institute for Energy- and Climate Research Troposphere (IEK-8), Research Center Jülich GmbH, Jülich, Germany
[4]Leibniz Institute for Tropospheric Research, Leipzig, Germany
[5]Department of Atmospheric Science, Colorado State University, Fort Collins, USA
[6]Department of Marine Earth and Atmospheric Science, North Carolina State University, Raleigh, USA

[7] Institute for Atmospheric and Climate Science, ETH Zürich, Zürich, Switzerland

Received: 11 February 2011 – Accepted: 25 February 2011 – Published: 2 March 2011

Correspondence to: P. Reitz (p.reitz@mpic.de)

Published by Copernicus Publications on behalf of the European Geosciences Union.

ACPD
11, 7235–7289, 2011

Abstract

The ability of coated mineral dust particles to act as cloud condensation nuclei (CCN) and ice nuclei (IN) was investigated at LACIS (Leipzig Aerosol Cloud Interaction Simulator) during the FROST1- and FROST2-campaigns (*Fr*eezing *o*f du*st*). Sulphuric acid was condensed on the particles which afterwards were optionally humidified, treated with ammonia vapour and/or heat. By means of aerosol mass spectrometry we found evidence that processing of mineral dust particles with sulphuric acid leads to surface modifications of the particles. These surface modifications are responsible for the observed reduction of the IN activation of the particles. The observed particle mass spectra suggest that different treatments lead to different chemical reactions on the particle surface. Possible chemical reaction pathways and products are suggested and the implications on IN and CCN efficiency of the treated dust particles are discussed.

1 Introduction

Aerosol particles have various direct and indirect effects on earth climate (Lohmann and Feichter, 2005). One of the important indirect effects is their ability to act as heterogeneous ice nuclei. Heterogeneous ice nucleation influences the earth radiation budget by the change of cloud albedo (Kay et al., 2007) and plays a major role in the formation of precipitation, especially in mid latitudes (Roedel, 2000). The exact effect of ice clouds on the Earth's climate is yet not well understood (Forster et al., 2007) and more research is needed to determine the mechanisms of heterogeneous ice nucleation (Cantrell and Heymsfield, 2005). Mineral dust has been found to be one of the major components of snow crystal residuals (Kamphus et al., 2010; Mertes et al., 2007; Richardson et al., 2007; Cziczo et al., 2004; DeMott et al., 2003). In the atmosphere mineral dust is often internally mixed with organic and inorganic material due to particle ageing processes in the atmosphere (Wiacek and Peter, 2009; Sullivan et al., 2007; Sullivan and Prather, 2007; Hinz et al., 2005; Falkovich et al., 2001). Such additions

ACPD
11, 7235–7289, 2011

may influence the efficiency of mineral dust to act as ice nuclei (Sullivan et al., 2010b,a; Niedermeier et al., 2010; Gallavardin et al., 2008; Möhler et al., 2008, 2005). Niedermeier et al. (2010) found that active sites are lost when particles are processed with concentrated sulphuric acid and Sullivan et al. (2010b) show that the loss of these active sites is irreversible. However, the surface processes that lead to the destruction of active sites are not fully understood. Here we present a study of reactions taking place on the particle surface of Arizona Test Dust after processing with sulphuric acid. The experiments were performed during the FROST1 and FROST2 (Freezing of dust 1 and 2) campaigns at the LACIS (Leipzig Aerosol Cloud Interaction Simulator, Hartmann et al., 2011; Stratmann et al., 2004) facility located at the Institute for Tropospheric Research in Leipzig, Germany. A unique combination of data from ice nucleus counters, a cloud condensation nucleus counter, and from aerosol mass spectrometers permitted deeper insights into the chemical processes taking place on the particle surface after processing with sulphuric acid. After condensing sulphuric acid on the particles, they were optionally humidified, neutralised and heated. These treatments and the resulting aerosol properties modifications provided additional information on the nature of the processes taking place on the aerosol particle surfaces. The possibility to link surface modifications to the modification of freezing behaviour is valuable for attaining greater understanding of the key characteristics that are responsible for the action of mineral dust particles as ice nuclei.

2 Methods

2.1 Particle generation

Arizona test dust (ATD) (ISO 12103-1, A1 Ultrafine Test Dust, Powder Technology Inc., Burnsville, Minnesota, USA) was chosen as test substrate. Additional measurements were performed using quartz particles (BCR-66, European commission, Institute for Reference Materials and Measurements). A schematic of the set-up is shown in Fig. 1.

ACPD
11, 7235–7289, 2011

It can be separated in two major blocks, the particle generation, shown on the left side of Fig. 1 and the particle characterisation, shown on the right side of Fig. 1. First, the ATD was dispersed in a fluidized bed generator (TSI 3400A, TSI Inc., St. Paul, Minnesota, USA). To generate aerosol with particles in the size range of 200 to 400 nm mobility diameter, ultra fine ATD was introduced into the disperser followed by a multi stage impactor with a 50% aerodynamic cut-off diameter at 560 nm (which corresponds to mobility diameter of approximately 450 nm) placed immediately after the fluidized bed, to remove most of the big particles prior to any processing. For those experiments with 400 nm mobilty diameter ATD, the impactor cut-off was increased to 1 µm corresponding to a mobility diameter of approximately 800 nm. The final selection of the aerosol diameter is performed at the end of the particle generation section. By passing the aerosol over a heated sulphuric acid bath, controlled amounts of sulphuric acid were condensed on the particle surface, depending on the temperature of the bath. More details can be found in Niedermeier et al. (2010).

Additional processing by humidification of the aerosol was accomplished using a water bath downstream of the sulphuric acid bath. We have indirect evidence that an unknown amount of ammonia was present in the compressed air and/or the water bath section. We were not able to quantify this contamination. It should be noted that the uptake of ammonia to the particles without water is very slow, meaning that only a very weak neutralisation could take place without the water bath in line. For some experiments extra ammonia was added to the aerosol in order to ensure complete neutralisation. After the water bath and the ammonia section, the aerosol was dried again in a diffusion dryer. Finally a thermodenuder was available in order to remove the semi-volatile fraction of the particles. Unavoidably, the thermodenuder, which was set most of the time to 250 °C, also provoked a thermal treatment of the aerosol in a way that surface reaction kinetics and equilibria might have been changed. At the end of the particle generation a differential mobility analyser (DMA) was used to select a monodisperse fraction of the aerosol of 200 nm, 300 nm or 400 nm mobility diameter. Doubly charged particle artefacts were mostly avoided as this size fraction had already

ACPD
11, 7235–7289, 2011

previously been removed by the impactor. As the 300 nm particles yielded the highest number concentration without doubly charged particles, they were used for most of the studies. Except for the DMA, all processing following the dispersion of the dust was optional and could be bypassed.

2.2 Particle characterisation

The aerosol was characterised with respect to concentration, morphology, hygroscopic growth, CCN activity, IN activity and chemical composition. In this paper we will focus on the results from the chemical analysis performed by an aerosol mass spectrometer (AMS) (Jayne et al., 2000; Drewnick et al., 2005) and compare the results to the CCN and IN activity measured by a cloud condensation nucleus counter (CCNC, Roberts and Nenes, 2005), an ice nucleus counter (CFDC, Sullivan et al., 2010b, original instrument version: Rogers et al., 2001) and the Leipzig Aerosol Cloud Interaction Simulator LACIS (Hartmann et al., 2011; Stratmann et al., 2004), which measured both CCN and IN efficiency. However, this study focuses on the IN data measured with LACIS. Data from an Aerosol Time of Flight Mass Spectrometer (ATOFMS) (Nordmeyer and Prather, 1994) was used to estimate the number-fraction of particles coated.

2.2.1 Determination of the particle soluble mass loadings from CCNC data

A detailed discussion of the hygroscopic growth properties of the probed aerosol is given in Wex et al. (2011). In the CCNC the supersaturation was varied in the range of 0.07 to 0.6% supersaturation and the number concentration fraction of activated particles was recorded. The supersaturation at which 50% of the particles were activated as cloud droplets was considered to be the critical supersaturation. As the aerosol is nearly monodisperse, the curves obtained show a relatively steep increase at a given supersaturation. To facilitate comparisons between AMS data and CCNC data, soluble mass loadings per particle have been calculated using single parameter Köhler theory (Petters and Kreidenweis, 2007; Wex et al., 2007). At the supersaturation S_{crit} at which

ACPD
11, 7235–7289, 2011

the particles activate, the maximum of the Köhler curve was calculated to determine the apparent hygroscopicity parameter κ_{app} which can then be compared to κ_{coat} of the pure substance used as the coating material. Equation (1) shows the Köhler equation linking the wet size D of a particle to the saturation ratio S needed.

$$S(D) = \frac{D^3 - D_{dry}^3}{D^3 - D_{dry}^3(1-\kappa_{app})} \exp\frac{A}{D} \quad (1)$$

D_{dry} is the dry diameter of the particle and A is a constant depending on the temperature and the surface tension at the solute/air interface. We use the term "apparent" hygroscopicity, as we determine the intrinsic hygroscopicity, biased by the possibly limited solubility of a fraction of the particle material (Sullivan et al., 2009b; Petters and Kreidenweis, 2008). The apparent hygroscopicity is the additive value of the apparent hygroscopicities of individual components of the particle weighted by their volume fractions. With κ_{coat} being the hygroscopicity parameter of the coating substance, κ_{ATD} being the hygroscopicity parameter of the unprocessed ATD and ϵ_{coat} and ϵ_{ATD} their respective volume fractions, we get Eq. (2) for κ_{app}:

$$\kappa_{app} = \epsilon_{coat}\kappa_{coat} + \epsilon_{ATD}\kappa_{ATD} \quad (2)$$

As the sum of the volume fractions must be equal to 1 ($\epsilon_{coat} + \epsilon_{ATD} = 1$), Eq. (2) can be rearranged to get the volume fraction of the coating (Sullivan et al., 2009a). This volume fraction can be multiplied by the particle volume and the density of the coating material, yielding the mass of the soluble fraction of the particle (Eq. 3). κ_{app} of the ATD was found to be 0.002 (Sullivan et al., 2010b).

$$\begin{aligned} m_{soluble} &= \rho_{soluble} \times V_{coat} \\ &= \rho_{soluble} \times V_{total} \times \epsilon_{coat} \\ &= \rho_{soluble} \times V_{total} \times \frac{\kappa_{app} - \kappa_{ATD}}{\kappa_{coat} - \kappa_{ATD}} \end{aligned} \quad (3)$$

ACPD
11, 7235–7289, 2011

This method works best if no reactions take place on the particle surface, as these can result in the formation of unknown substances for which the hygroscopicity parameter and the density are no longer exactly known.

2.2.2 Determination of IN efficiency

The CFDC is a continuous flow diffusion chamber. The dry aerosol is cooled down and enters a region between two cylinders which are coated with ice and set to a controlled temperature. By creating a temperature gradient between the cylinder walls, the saturation ratio between the walls can be controlled. Particles which activate and grow to ice crystals are counted with an optical particle counter at the end of the chamber. The instrument can measure both in immersion/condensation freezing mode (particles activate as cloud droplets before freezing) as well as in deposition freezing mode (water vapour directly deposits on the particles to form ice without prior activation of the particles as liquid droplets). The different freezing modes are described in Pruppacher and Klett (1997). Details about the CFDC chamber used during the FROST2 campaign are described in Sullivan et al. (2010b).

In the LACIS chamber, moisture conditioned aerosol is cooled down in a laminar flow tube in order to achieve supersaturation above water. The supersaturation and the temperature of the aerosol are controlled via the wall temperatures and the initial air moisture. Downstream of the activation of the particles to droplets, further cooling occurs, that can eventually lead to the freezing of the droplets. At the outlet an optical particle counter is used to detect the ice and the droplets formed. Ice is formed in the immersion freezing mode. Details about the LACIS chamber and its use as an ice nucleation instrument are given in Hartmann et al. (2011).

ACPD
11, 7235–7289, 2011

2.2.3 Determination of the chemical composition of the particles' non refractory fraction

In the AMS particles of 40 nm to 1000 nm vacuum aerodynamic diameter are focused on a narrow particle beam using an aerodynamic lens. 100% transmission is achieved for particles in the range from 60 nm to 600 nm vacuum aerodynamic diameter (Liu et al., 2007). The focused particle beam is introduced into a differentially pumped vacuum chamber and directed onto a thermal vaporiser whose temperature was set to 600 °C or 820 °C. The use of two different evaporation temperatures provided additional information on the volatility of the particle material, allowing further restricting its possible composition. The produced vapour is ionized by 70 eV electron impaction and the positive ion fraction is focused into an orthogonal extraction time-of-flight mass spectrometer.

The main objective of the AMS measurements was to quantify the amount of sulphuric acid condensed on the particle surface. The temperatures set at the AMS vaporiser are far too low to evaporate mineral dust like ATD (melting point according to manufacturer: 1615 ± 75 °C). Nevertheless, the instrument is sensitive to the more volatile fraction of the particles, thereby facilitating the detection of even very low amounts of non-refractory material on the refractory particle cores. As the aerosol was quasi monodisperse, the average mass per particle could be calculated by normalising the mass concentrations given by the AMS to the particle number concentration from a condensation particle counter (CPC) that was operated parallel to the AMS.

In the following paragraphs the determination of necessary correction factors is described. They cover the relative ionisation efficiency of the sulphate species which is determined by an additional calibration to ammonium sulphate, the correction for the collection efficiency of particles on the vaporiser, which is lower than unity due to bounce off effects, the transmission of the aerodynamic lens, and the determination of a comparability factor due to accumulated measurement uncertainties from different instruments when comparing the FROST1 to the FROST2 campaign.

ACPD
11, 7235–7289, 2011

In order to make the quantification of sulphate compounds as accurate as possible, the instrument was calibrated using ammonium sulphate, in addition to the ammonium nitrate calibration (Jayne et al., 2000). A known issue of the AMS quantification is the bounce off of particles from the vaporiser prior to their evaporation, lowering the collection efficiency (CE) of the instrument and thus resulting in underestimation of the measured mass (Huffman et al., 2005; Matthew et al., 2008). An estimation of the collection efficiency of mineral dust like particles coated with sulphuric acid was achieved by measuring quartz particles (BCR-66) in the same size range with different sulphuric acid coating thicknesses parallel to a CCNC. As the surface of quartz particles does not react with sulphuric acid, the amount of sulphuric acid on the particles could be determined from CCNC measurements as described above, assuming that all of the soluble material is composed of sulphuric acid. By comparing the mass deduced from the AMS data to the amount of soluble mass, the collection efficiency was determined. The quartz particles showed a small amount of soluble material even without coating, thus contained small amounts of soluble impurities. Note that BCR-66 is not a chemical standard but a size standard. However, these were the best quartz dust samples in the size range needed which were commercially available. Figure 2 shows a compilation of the ratios between AMS and CCNC mass per particle for all experiments performed in order to determine the CE. Its average value is 0.357 ± 0.022. The average value was used in the correction of the mass per particle as it seems very unlikely that the CE would change due to coatings in the order of magnitude of 1 nm.

The particles most extensively characterised in these studies had a mobility diameter of 300 nm, corresponding to a vacuum aerodynamic diameter of about 600 nm. This is at the 100% transmisson edge of the aerodynamic lens. Due to an aerodynamic shape factor variability of the ATD particles, the monodisperse aerosol with respect to its mobility diameter is polydisperse with respect to its vacuum aerodynamic diameter. This causes a fraction of the particles to be outside of the 100% transmission range of the aerodynamic lens. For the 400 nm particles this effect is even more pronounced. In order to get accurate mass loadings, this extra loss factor was estimated. Because

ACPD
11, 7235–7289, 2011

the low amounts of non-refractory material on the particles produced noisy size distributions and the size calibration above 600 nm is imprecise, some assumptions were made: The vacuum aerodynamic mass size distribution of the ATD was assumed to be lognormally distributed with the same geometric width independent of the mode diameter (Fig. 3). The lognormal fit to the 200 nm particles which are fully within the 100% transmission range of the aerodynamic lens, can be projected to the 300 and 400 nm particles. For that we take advantage that the vacuum aerodynamic diameter d_{va} and the mobility diameter d_{mob} are linearly linked by the "Jayne shape factor" S and the particle density ρ_p (Eq. 4, DeCarlo et al., 2004; Jayne et al., 2000). S was determined to approximately 0.77 and the density of the ATD is 2.6 g cm^{-3} (Möhler et al., 2008). ρ_0 is the unit density (1 g cm^{-3}).

$$d_{va} = S\frac{\rho_p}{\rho_0}d_{mob} \tag{4}$$

The mass size distributions were calculated from the methyl silicone signal, as this substance showed the best signal to noise ratio. The presence of this substance on the particle surface will be discussed in more detail in Sect. 3.1. A second assumption was that the transmission function f_{trans} of the aerodynamic lens for ATD and BCR-66 particles is identical to that of polystyrol latex size standards (PSL) which where used to determine the transmission function during laboratory measurements (S. Walters, personal communication, 2008). Finally the integral of the projected mass size distribution D_{ATD} was divided by the integral of the product of the transmission function and the projected mass size distribution resulting in a correction factor k_{trans} for the lens transmission (Eq. 5). The respective projected distributions are shown in Fig. 4. The correction factors are shown in Table 1.

$$k_{trans} = \frac{\int_0^{+\infty} D_{ATD}(d_{va})dd_{va}}{\int_0^{+\infty} D_{ATD}(d_{va}) \times f_{trans}(d_{va})dd_{va}} \tag{5}$$

When comparing the FROST1 to the FROST2 campaign, the mass per particle loadings were not well reproduced for similar settings in the particle generation section.

ACPD
11, 7235–7289, 2011

Possible reasons for these discrepancies are the accuracy of the CPC concentrations to which the AMS data was normalised (10%), the dilution stage in front of the CPC (10%), as well as the accuracy of the AMS calibration (30%). After gaussian error propagation, with the AMS and the CPC error counted twice as it is present for both campaigns, this yields an uncertainty of 46%. Other sources are speculative but can not be excluded. The dilution factor was close to 5 which means that small measurement errors in the dilution flow are highly amplified when calculating the particle number concentrations before dilution from the CPC counts and thus the mass loadings are highly sensitive to the flow measurement. We performed supplementary experiments with only the CCNC, the AMS and a CPC without dilution. In these measurements the CCNC activation curves matched those of the experiments done with the same parameters during FROST1 and FROST2. By adjusting the AMS mass loadings of the FROST 1 and 2 campaign to the data of these experiments, the FROST campaign data were corrected for these systematic errors. The factors also make the BCR-66 calibration measurements comparable to the ATD measurements during the campaigns. Table 2 shows these comparability factors.

The AMS is calibrated by measuring a known quantity of ammonium nitrate in order to determine the ionisation efficiency (IE) of the instrument for the nitrate fragments at the mass to charge ratios 30 (NO^+) and 46 (NO_2^+). The IE of other species differ from the IE of nitrate and thus relative ionisation efficiencies (RIE) have to be determined for each species (e.g., Alfarra et al., 2004). The RIE values of sulphate and ammonium, which were determined separately for each campaign, are given in Table 3.

In addition to the AMS, an Aerosol Time of Flight Mass Spectrometer (ATOFMS; TSI Model 3800) was used in this study to determine aerodynamic size and chemical composition of single particles. It uses an aerodynamic sizing technique to measure particle size and time of flight mass spectrometry to determine the chemical composition of particles of unit mass resolution. Particles in the size range between approximately 200–3000 nm are drawn into the instrument through a nozzle inlet and are first aerodynamically sized by measuring their transit time in between two laser beams of

ACPD
11, 7235–7289, 2011

known distance. Downstream of the sizing region, the particles reach the ion source region where the particles are hit by pulsed UV laser fires that induces laser desorption/ionisation. Due to the bipolar design of the mass spectrometer, a positive and a negative ion spectrum are acquired from each particle.

The main differences compared to the AMS are the capability of the ATOFMS to analyse single particles, as well as to collect information on refractory materials such as sodium chloride, elemental carbon and mineral dust constituents due to the different ionisation method applied. However, compared to the AMS, the ATOFMS does not measure mass concentrations. A common method to analyse ATOFMS spectra is to classify analysed particles into groups of certain mass spectrometric signatures which was also done in the context of this experiment. Herein, we queried single particles mass spectra for a peak at $m/z = -97$ which is a clear marker for sulphate. Applying different peak thresholds (conservative: peak area >1000 a.u.; less conservative: peak height >50 a.u.), the number fraction of particles that produce a sulphate ion signal could be determined.

3 Results and discussion

The presentation of the results starts with the identification of chemical compounds found in the non-refractory fraction of the ATD followed by the quantification of the average mass per particle for the main species. We show evidence for reactions of the sulphuric acid with the particle surface and propose possible products from these reactions depending on the applied treatments. The mass per particle loadings, as deduced from the AMS data, are compared to the soluble mass fractions calculated from the CCNC activation curves. This comparison allows for further restricting the possible products on the particles' surface. Finally, the effects of the different treatments are linked to the IN-fractions determined by the CFDC and LACIS, to show their effects on the IN-ability of ATD.

ACPD
11, 7235–7289, 2011

In general, for all particles the mass per particle was calculated for the species organics, sulphate, ammonium and silicone. The detection limits have been calculated from the amplitude of the noise of the background signal similar as in Drewnick et al. (2009) using an algorithm described in Reitz and Schneider (2011) to separate long scale background fluctuations from statistic noise. The correction factors described in Sect. 2 were applied to all species.

3.1 Average non-refractory mass per particle

The average non-refractory mass per particle was determined by normalising the mass concentrations of carbon containing material (CCM), sulphate, ammonium and silicone measured with the AMS to the particle number concentration measured by a CPC. The term CCM was introduced instead of the term organics, as it also contains carbonates and methyl silicone, which cannot be clearly distinguished from organic material. The fragmentation table is the same as for organics (Allan et al., 2004). The ATOFMS data show that 84 to 97% or 93 to 100% of the particles contained sulphate after passing the sulphuric acid coating section. The numbers depend on the signal area threshold used. Based on the signal quality of the individual mass spectra, the less conservative threshold can be applied for the investigated experiments. However, sulphate peaks were also detected for "pure" ATD particles, which makes the identification of sulphate compounds on the particles somewhat ambiguous. The fraction of pure ATD particles that showed a sulphate peak ranges from 3 to 8% and 5 to 46% using similar threshold definitions as described above. The fact that a small fraction of the coated particles showed no sulphate peak in the ATOFMS likely could be related to the very low amounts of sulphate on the particle surface. Due to this it is possible that even when sulphate was present, it did not necessarily produce a significant signal in the ATOFMS. The CCNC data also indicated that the aerosol was not externally mixed, as the activation of the particles took place in a small supersaturation interval without showing multiple steps, as would have been expected in case of an uncoated fraction. A compilation of the coated particle fraction determined with the ATOFMS is shown in Table 4.

ACPD
11, 7235–7289, 2011

Figures 5a to 5c show average mass spectra recorded during the FROST1 and FROST2 campaign. No correction factors have been applied for these graphs. Figure 5a shows the data measured using ATD without sulphuric acid processing. Beside the two clear silicone peaks, only organic material is visible, especially on the mass to charge ratios (*m/z*) 55, 56 and 57 which are clearly organic markers. Figure 5b shows pure ATD from the FROST2 campaign, during which the vaporiser temperature was increased by 220 °C compared to FROST1. The high temperature leads to a stronger decomposition of the oxygenated organics and the decomposition of carbonates (see extensive study by Zhao et al., 2010), resulting in a rise of the CO_2^+ fragment. The signal on *m/z* 57 indicates the presence of organic material that has not been as heavily decomposed by the high temperature. A second effect of the high vaporiser temperature is the appearance of alkali metal peaks (Na^+,K^+,Rb^+ and Cs^+) as well as Ba^+, the stable alkaline earth metal with the lowest electronegativity. These peaks only appear when ATD is introduced into the instrument and are missing during e.g. calibration measurements with ammonium nitrate. It is possible that a low amount of alkali metals from the ATD were surface ionised (Svane et al., 2004, 2005). Given their very low electronegativity they are extremely easily ionised and low amounts would already produce high signals. The analysis of ATD in Vlasenko et al. (2005) did only show Na^+ and K^+ of these metals, but others might have been below the detection limit of the X-ray photo-electron spectroscopy used for this analysis or not included at all. The silicone signal which was identified in FROST1 is also present in the FROST2 data and the BCR-66 measurements. Figure 5c originates from a FROST2 measurement with sulphuric acid bath temperature of 70 °C with an average sulphate mass of 1.870×10^{-12} µg/particle. The resulting sulphate peaks are marked in red. The silicone peaks are no longer visible in this data. We suppose that they were oxidised by the sulphuric acid. The metal peaks remain, as expected for the vaporiser temperature of 820 °C.

ACPD
11, 7235–7289, 2011

Figures 6a to 6c show a summary of the mass per particle for all experiments of the FROST campaigns with all correction factors applied. In Fig. 6a, the first three entrees show pure particles with 200, 300 and 400 nm mobility diameter. Only CCM is found on the surface including methyl silicone, which is plotted additionally on the right axis. The source of the silicone is probably silicone grease or oil which is often used in pumps. We are unable to tell whether it was already on the ATD surface before our treatments, or if it was introduced by our system. We could however exclude conductive black silicone tubing as a direct source, as has been found by Timko et al. (2009),Yu et al. (2009), and Schneider et al. (2006), because the set-up used only stainless steel tubing. It is most likely that the silicone contamination is not relevant for the freezing and droplet activation behaviour in these experiments, as the amount of silicone is by far too low to produce a layer on the particle surface that could cover a significant fraction of active sites. We also do not expect it to produce active site on its own, as it is amorphous and hydrophobic and thus is very unlikely to trigger the formation of a crystalline structure from water. The main interest of this substance was its excellent signal to noise ratio, making it possible to retrieve size distributions for the pure ATD.

In the sulphuric acid condensation section, sulphuric acid condensed on the particle surface and its amount increased with higher temperature of the sulphuric acid reservoir as well as with the increase of the particle surface area. The amount of CCM was reduced by the sulphuric acid, which can displace carbonate from its salts as well as react with organic substances. The methyl silicone signal vanishes almost completely at high sulphuric acid bath temperatures. Due to chemical reactions with the particle surface we expect the formation of iron, aluminium, and calcium containing sulphate salts, as these metals have been found with high abundance on the ATD surface as shown in Table 5 based on Vlasenko et al. (2005). For all species the increase of the mass per particle is proportional to the surface area of the particles, indicating that most of the material was evaporated from the particle surface.

The addition of ammonia was accompanied by humidification of the particle surface. The first effect of the particle humidification was the improved uptake of ammonia

ACPD
11, 7235–7289, 2011

and thus the neutralisation of the sulphuric acid. In addition, the humidity provoked a stronger reaction of the sulphuric acid with the particle surface, which competed with the neutralisation process. The reaction of the particle surface resulted in the formation of metal sulphate salts, which partly could not be evaporated by the vaporiser of our instrument at 600 °C. Evidence for the consumption of a significant fraction of the sulphuric acid prior to its neutralisation is given by the mass spectra discussed in Sect. 3.2 and shown in Fig. 8a and Fig. 8b. During FROST2, the vaporiser temperature was set to 820 °C, thereby facilitating the evaporation of metal sulphate salts which could not be detected during FROST1.

Figure 6b shows the average mass loadings for pure ATD particles and ATD particles with low amounts of sulphuric acid condensed on their surface during FROST2. The first four categories show uncoated particles. In the first category, the thermodenuder was turned off. This data point can be compared to the FROST1 uncoated 300 nm particles. The silicone mass matches very well the FROST1 findings, however the CCM mass is higher by more than a factor of two, as carbonates were decomposed by the higher vaporiser temperature. With the temperature of the thermodenuder increasing, the silicone was systematically reduced, whereas the amount of CCM did not show any clear trend. The three categories on the right show experiments with a low amount of condensed sulphuric acid. As in the FROST1 data, the sulphuric acid reduced the CCM. The use of the thermodenuder did not have any clear effect on the CCM mass, whereas the sulphuric acid was already clearly reduced when the thermodenuder was set to 45 °C. Additional increase of the thermodenuder temperature to 250 °C did not affect the sulphate signal further. This effect can also be seen in Fig. 6c for the data points at 70 °C sulphuric acid bath temperature. There is no significant difference between the measurement with the denuder temperature of 70 °C and 250 °C. In Sect. 3.2 it is shown that the higher temperature mainly results in a more efficient reaction of the sulphuric acid with the particle surface.

ACPD
11, 7235–7289, 2011

3.2 ATD surface reactions

Analysing the effects of the thermodenuder and applying the water bath gave insight into the possible reactions taking place on the particle surface. For that we analysed the mass per particle and the fragmentation pattern. Figure 7 shows the expected fragmentation for sulphuric acid, ammonium sulphate and metal sulphate salts. Only sulphuric acid and ammonium sulphate can produce the hydrogen containing fragments HSO_3^+ and $H_2SO_4^+$, which can not be formed from metal sulphate salts. This difference is clearly visible in the fragmentation patterns shown in Figs. 8a and 8b, depending on the treatment of the particles. The use of the water bath, independent on the addition of NH_3 and the use of the thermodenuder strongly reduced the hydrogenated fragments. It can be concluded that in both cases the reaction with the particle surfaces was enhanced, thereby resulting in the production of metal sulphate salts. The thermodenuder had a stronger effect on the mass per particle when it was used alone compared to its use after the water bath. The reason likely is that the water bath also caused the neutralisation of the sulphuric acid to be more effective, as the uptake of ammonia was expected to be improved on a wet particle. This hypothesis is based on the elevated ammonium signal from those particles coated with a sulphuric acid bath temperature of 85 °C with the water bath in use. Deliberately adding further ammonia to the air did not influence the ammonium signal significantly. The ammonium measured for these experiments corresponds to 0.51 ± 0.12 times the concentration necessary for a complete neutralisation of the sulphuric acid. However, when the thermodenuder was used after the water bath, the ammonium signal was reduced by at least a factor of 2. For all other experiments the ammonium could not be quantified as the ammonium signal was too small compared to the interference by air ions. It was not possible to correct for these interferences because the standard correction method via a fragmentation table as described in Allan et al. (2004) was not applicable as these corrections are based on the assumption of a stable ratio between oxygen and nitrogen. This was not the case for these experiments, limiting reliable

ACPD
11, 7235–7289, 2011

statements about the quantities of ammonium to those experiments with a relatively high amount of ammonium. However, we expect that for those experiments using the water bath, for which we could not quantify the ammonium, the effect is similar to the 85 °C sulphuric acid bath temperature experiments. The addition of ammonia gas did not significantly influence the neutralisation, which indicates that the carrier air used in the system already contained enough ammonia for a partial neutralisation and/or the branch after the water bath was contaminated with ammonia. We expect that the partially neutralised sulphuric acid can produce mixed ammonium sulphate metal salts, which can still be evaporated in the AMS, but at the lower temperatures of the thermodenuder only a partial decomposition could take place, which liberated ammonia but not sulphur oxide. We propose that the following reactions are responsible for the difference between the experiments with sulphuric acid processed particles without further treatment and those experiments with water bath and/or thermodenuder. The actual chemistry may be much more complex and part of the reactions shown below for one category will also take place in other categories. In order to improve readability, the reactions are only shown for a generic metal M with valency of 3 (e.g. Al or Fe(III)) and assuming that the mineral includes carbonate. They can be easily rewritten with metals with a different valency (e.g.: K, Ca or Fe(II)) or combinations of different metals and with different anions (e.g. OH^- or PO_4^{3-}). The equations are not equilibrated as we do not know the relative quantities of the reaction products. The liberation of ammonia as proposed in Reaction (R7) is based on the reduced ammonium signal when the thermodenuder is used after the water bath for the experiments with the sulphuric acid bath at 85 °C and the decomposition temperatures as indicated in Table 5. (g) indicates that the substance is present in the gas phase after the process and SO_i represents sulphur oxides:

water bath only:

ACPD
11, 7235–7289, 2011

$$M_2(CO_3)_3 + H_2SO_4 + NH_3 \xrightarrow{H_2O} M_2(SO_4)_3 + MNH_4(SO_4)_2 + (NH_4)_2SO_4 + CO_2(g) + H_2O(g) \quad \text{(R1)}$$

$$\xrightarrow{\text{vaporiser}} M_2O_3 + NH_3(g) + SO_i(g) + H_2SO_4(g) + H_2O(g) \quad \text{(R2)}$$

Thermodenuder only:

$$M_2(CO_3)_3 + H_2SO_4 \xrightarrow{250^\circ C} M_2(SO_4)_3 + CO_2(g) + H_2O(g) \quad \text{(R3)}$$

$$\xrightarrow{\text{vaporiser}} M_2O_3 + SO_i(g) \quad \text{(R4)}$$

Water bath followed by the thermodenuder:

$$M_2(CO_3)_3 + H_2SO_4 + NH_3 \xrightarrow{H_2O} M_2(SO_4)_3 + MNH_4(SO_4)_2 + (NH_4)_2SO_4 + CO_2(g) + H_2O(g) \quad \text{(R5)}$$

$$\xrightarrow{250^\circ C} M_2(SO_4)_3 + M(HSO_4)_3 \quad \text{(R6)}$$

$$+ NH_3(g) + H_2O(g) + SO_i(g) \quad \text{(R7)}$$

$$\xrightarrow{\text{vaporiser}} M_2O_3 + H_2O(g) + SO_i(g) \quad \text{(R8)}$$

3.3 Comparison of non refractory mass loadings to soluble mass loadings

In Fig. 9 the soluble mass per particle, calculated from the CCNC data as described in Sect. 2.2.1, is plotted versus the sulphate mass per particle measured with the AMS. The amount of soluble mass was calculated under the assumption that it was composed of sulphuric acid. This assumption was made for simplification as we do not exactly know which substances have been created on the particle surface by reaction

ACPD
11, 7235–7289, 2011

of sulphuric acid with the ATD particles. The graph shows a linear relation between the soluble mass and the non-refractory mass at 600 °C, except for one point. The point marked "outlier", which is located away from the linear fit, was an experiment with the water bath in use during the FROST1 campaign. It showed no hydrogenated sulphate fragments at all. The reduction of the hydrogen containing fragments indicates that the reaction with the particle surface was accelerated, most likely producing more material which is soluble but cannot be evaporated at 600 °C, as described in Sect. 3.2, and can therefore not be detected by the AMS. This data point indicates a chemical modification of the particles by the use of the water bath but further study of this system is needed to confirm this hypothesis.

Figure 10 shows the comparison of soluble mass to AMS sulphate mass per particle for the FROST2 campaign. As already mentioned, during this campaign, the temperature of the AMS vaporiser was set to 820 °C which was 220 °C higher than during FROST1. This allows for the vaporisation of additional substances compared to FROST1. The graph shows that with the higher temperature all experiments show a linear relation between CCNC and AMS.

The slope of the fit curve for both comparison graphs is the same within the error (FROST1: 0.75; FROST2: 0.64) due to the 30% calibration accuracy of the AMS. This indicates that the material produced by chemical reaction on the particle surface without the water bath could already be completely evaporated at 600 °C, while the material produced with the water bath must have a higher vaporization temperature than the reaction products without water bath. No thermodenuder experiments were performed during FROST1 but a similar effect than with the water bath can be expected for the different denuder temperatures. Substances that were produced without the water bath could be iron(II)- and iron(III)sulphate. Candidates for the additional compounds produced with the water bath are aluminium sulphate and calcium sulphate. As shown in Table 5, all three metals can be found on the ATD surface in relatively high abundance. The iron sulphate salts decompose at 400 °C and 480 °C while aluminium sulphate decomposes at 770 °C and calcium sulphate at 700 °C (IFA, 2010). It is possible to

ACPD
11, 7235–7289, 2011

detect iron sulphate salts in the AMS with a vaporiser temperature of 600 °C but for aluminium sulphate more than 770 °C and for calcium sulphate more than 700 °C are necessary in order to get flash decomposition of these substance. In Table 5 a more extensive list of possible reaction products is shown together with their respective decomposition temperatures and their solubility. For some substances the table contains the melting temperature, as this temperature corresponds in good approximation to the evaporation temperature under high vacuum conditions prevailing in the AMS. This list of compounds is of course not complete, as a lot of other reaction products are possible on the ATD surface. The table shows that all compounds except $CaSO_4$ have a solubility higher than 100 g l^{-1} indicating that all of these substances contributed to the apparent hygroscopicity determined with the CCNC (Sullivan et al., 2009b; Petters and Kreidenweis, 2008). Considering the data point with humidification by the water bath in Fig. 9, we cannot explain its behaviour with the formation of $CaSO_4$ e.g. from $CaCO_3$ as $CaSO_4$ is not soluble enough to be measured with the CCNC (details in Wex et al., 2011). However this does not exclude that $CaSO_4$ was formed too. The additional formation of $Al_2(SO_4)_3$ from e.g. $AlPO_4$ could explain this behaviour. From the ATD analysis by Vlasenko et al. (2005) we know that small amounts of phosphate can be found in ATD. Possible precursors of $Al_2(SO_4)_3$ could also be minerals containing OH^- anions. The proposed reactions are all based on the material available. Reliable conclusions on the exact chemistry of the surface reactions need more investigations, especially to directly identify the products of the reactions.

3.4 Effect of particle surface modification on IN ability

In this section the number of IN is linked to the results of the AMS data as shown in Figs. 11 and 12. More details about the evaluation and interpretation of the IN data is presented in Sullivan et al. (2010b) (CFDC) and Niedermeier et al. (2010) (LACIS). Both graphs illustrate that the number of IN was reduced with increasing amounts of sulphate per particle. In Fig. 11 the ice fraction was measured with the CFDC at 105% relative humidity with respect to water and a freezing temperature of −30 °C.

ACPD
11, 7235–7289, 2011

With these parameters, the analysed freezing mode was condensation or immersion freezing, meaning that the particles activated as liquid cloud droplets prior to freezing. The experiments with the water bath in use show a lower fraction of IN than experiments with the same amount of sulphate mass on its surface but without the water bath. In Sect. 3.2 we showed that when the particles were humidified by the water bath, no free, unreacted sulphuric acid was left on the particle surface. The sulphuric acid either reacted with the surface itself or was neutralised by the uptake of ammonia. Therefore it can be concluded that the main reason for the reduction of the IN fraction in the immersion/condensation freezing mode is not the coverage of the particle surface with sulphuric acid, but a chemical modification of the surface.

This hypotheses is supported by the comparison of the AMS mass loadings to the IN fractions calculated from the LACIS data shown in Fig. 12. All the data from LACIS refer to immersion freezing. For the particles with no treatment after the condensation of sulphuric acid, the IN fraction was reduced when the amount of sulphate was increasing. If the water bath is used, the IN fraction is reduced by one order of magnitude. This is in accordance with the finding in Sect. 3.2 where we showed that the use of the water bath reduced the intensity of those sulphate fragments that are typical for the presence of sulphuric acid. Using the thermodenuder has a similar but stronger effect. The thermodenuder however not only accelerated the surface reactions but it also removed part of the semi-volatile material. This has to be taken into account when interpreting those experiments where the thermodenuder was used after the water bath. The thermodenuder has no significant effect on the IN fraction when used after the water bath. It only reduces the sulphate mass on the particle surface to about 70%, moving the points on the graph to the left by a factor of approximately 1.5. As all of the coating material has already reacted with the surface or was neutralised due to the improved ammonia uptake on the wet particles, no sulphuric acid is left which could further attack active sites due to the heat treatment. Niedermeier et al. (2011) cover more details about the behaviour of the IN fraction and show data for different freezing temperatures in the LACIS chamber.

ACPD
11, 7235–7289, 2011

The reduction of the IN-efficiency of ATD through the reaction with sulphuric acid can be explained by the following hypothesis:
the nucleation ability of mineral dust to act as ice nuclei is thought to be linked to surface active sites (Vali, 1985) which may provide a structure similar to that of ice (i.e.: cubic or hexagonal ice), thereby lowering the energy barrier for ice formation to be initialised. Experiments performed by Choi et al. (2005) indicate that local electric fields present on the particle surface could also act as active sites. However, different active site properties not stated here are also possible as the nature of active sites is still not identified. Sullivan et al. (2010b) showed that the ATD IN-efficiency is irreversibly altered by the processing with sulphuric acid. We believe that through reaction with sulphuric acid, active sites are destroyed by etching, leaving a particle surface which no longer reduces the ice nucleation energy barrier efficiently, for example because it resembles the ice lattice structure less. This hypothesis implies that the material forming the active sites can react with sulphuric acid, which reduces the possible compounds or mixtures of compounds responsible for the ATD IN-behaviour. The substances additionally formed when the water bath or the thermodenuder was used were likely to contain calcium and aluminium. In future laboratory studies it would therefore be interesting to analyse pure aluminium and calcium containing minerals which can be etched by sulphuric acid. As we found that carbonates have been destroyed by the sulphuric acid, it is possible that carbonates are involved in the ice formation as suggested by Klein et al. (2010); Zimmermann et al. (2008); Mason and Maybank (1958), and Manson (1957). The comparison of the AMS non refractory mass at 600 °C to the soluble mass from the CCNC, indicates that the destruction of aluminium and phosphates or hydroxide containing minerals could also be involved in the chemical processes on the particle surface. Whether the destruction of such substances is linked to the destruction of the IN ability of ATD or not cannot be determined from these experiments and other compounds which we were unable to identify may also be responsible for the observed effect.

ACPD
11, 7235–7289, 2011

The humidification of the particle transforms the sulphuric acid on the surface to a highly concentrated sulphuric acid solution with the particle core immersed. This allows for two possible explanation for the effect of the water bath. First, the sulphuric acid could have been spread over the whole particle and thus became able to etch all active sites on the ATD surface, including those that were not in contact with the sulphuric acid if the particle surface was not completely covered after the condensation process. A second possibility is that the particles were already completely covered after the condensation of the sulphuric acid and the humidification only accelerated the reaction kinetics and/or changed the reaction equilibrium. However, the thermodenuder is only capable of changing the reaction equilibrium or the kinetics and no spreading of the sulphuric acid over the particle surface is expected. Nevertheless, the thermodenuder had a similar and even stronger effect to the IN-efficiency than the humidification. This indicates that the particle surfaces were already completely covered after the sulphuric acid condensation process as otherwise the thermodenuder would not have improved etching of the surface as efficiently. We therefore conclude that the reduction of the IN-fraction by the humidification is also due to reaction equilibrium or kinetics change as the whole surface must already have been covered by sulphuric acid prior to the humidification.

4 Summary and conclusions

It has been shown that condensing sulphuric acid on the ATD surface does not only coat the particles but also leads to surface reactions. The compounds produced on the surface were metal sulphate salts, ammonium metal sulphate salts as well as ammonium sulphate. The formation of metal sulphate salts was indirectly detected via the fragmentation pattern of the AMS sulphate signal. A direct detection was not possible as the metal oxides produced during the vaporisation process in the AMS are refractory. In our experiments the source of the ammonium was the intrinsic ammonia contained in the compressed air, a possible contamination of the water bath section

ACPD
11, 7235–7289, 2011

as well as ammonia that was on purpose added to the system to get full neutralisation. The amount of ammonium produced could not be quantified by the AMS, as the addition of ammonia together with nitrogen perturbed the ratio between oxygen and nitrogen in the compressed air, making it impossible to accurately correct for interferences between ammonium, water and oxygen. These problems can be avoided in future studies by the use of synthetic air and addition of ammonia mixed with this same composition of synthetic air.

Comparing the AMS data to the CCNC data for particles humidified or treated thermally after the coating with sulphuric acid yields evidence for the formation of an increased amount of substances which were evaporated by the AMS vaporiser at 820 °C but not at the lower temperature of 600 °C. However, the solubility of the surface material is altered only weakly. Possible compounds would be aluminium sulphate and calcium sulphate. The comparison of the AMS sulphate signal and the sulphate fragmentation to the IN fractions measured with the CFDC and LACIS show that the IN ability is reduced by the coating with sulphuric acid through reaction with the surface for the condensation/immersion freezing mode.

Coating the particle with sulphuric acid without further treatment slightly lowered the fraction of IN in the immersion/condensation freezing mode, while humidification after the coating and thermal treatment caused the IN-fraction to further decrease. The reduction of the IN fraction was attributed to the destruction of surface active sites as already proposed by Sullivan et al. (2010b). The condensation of sulphuric acid on the particle surfaces and the resulting reaction decreased the IN ability. The substances formed were vaporised at 600 °C in the AMS. The use of the water bath further decreased the number of IN and produced substances with lower volatility and lower solubility. The newly formed substances could only be evaporated at 820 °C. A similar but stronger effect was produced by the use of the thermodenuder if it was not preceded by the water bath. If the water bath was used before the thermodenuder, the thermodenuder effect was reduced to the removal of the volatile fraction of the particle. Aluminium and calcium containing minerals are likely part of the active sites. We

ACPD
11, 7235–7289, 2011

observed that the sulphuric acid reduced the amount of carbonates on the particles, indicating that they could be involved in the active site compounds (Klein et al., 2010; Zimmermann et al., 2008; Mason and Maybank, 1958; Manson, 1957). However further research is needed to clearly identify the chemical nature of the active sites.

Acknowledgements. This work was conducted within the Helmholtz virtual institute on aerosol cloud interaction and supported by the Integration of European Simulation Chambers for Investigating Atmospheric Processes (EUROCHAMP) program as well as by the US National Science Foundation (Grant ATM-0611936). We thank all the participants of the FROST campaigns for their support and valuable discussions.

The service charges for this open access publication have been covered by the Max Planck Society.

References

AlfaAeser: Data sheet ammonium iron(III) sulphate, http://www.alfa-chemcat.com/ (last access: March 2011), 2010. 7272

Alfarra, M. R., Coe, H., Allan, J. D., Bower, K. N., Boudries, H., Canagaratna, M. R., Jimenez, J. L., Jayne, J. T., Garforth, A. A., Li, S. M., and Worsnop, D. R.: Characterization of urban and rural organic particulate in the lower Fraser valley using two aerodyne aerosol mass spectrometers, Atmos. Environ., 38, 5745–5758, doi:10.1016/j.atmosenv.2004.01.054, 2004. 7246

Allan, J. D., Delia, A. E., Coe, H., Bower, K. N., Alfarra, M. R., Jimenez, J. L., Middlebrook, A. M., Drewnick, F., Onasch, T. B., Canagaratna, M. R., Jayne, J. T., and Worsnop, D. R.: A generalised method for the extraction of chemically resolved mass spectra from aerodyne aerosol mass spectrometer data, J. Aerosol Sci., 35, 909–922, doi:10.1016/j.jaerosci.2004.02.007, 2004. 7248, 7252

Cantrell, W. and Heymsfield, A.: Production of ice in tropospheric clouds - A review, B. Am. Meteorol. Soc., 86, 795, doi:10.1175/bams-86-6-795, 2005. 7237

Choi, E. M., Yoon, Y. H., Lee, S., and Kang, H.: Freezing transition of interfa-

ACPD

11, 7235–7289, 2011

cial water at room temperature under electric fields, Phys. Rev. Lett., 95, 085701, doi:10.1103/PhysRevLett.95.085701, 2005. 7258

Cziczo, D. J., Murphy, D. M., Hudson, P. K., and Thomson, D. S.: Single particle measurements of the chemical composition of cirrus ice residue during CRYSTAL-FACE, J. Geophys. Res.-Atmos., 109(13), D04201, doi:10.1029/2003jd004032, 2004. 7237

DeCarlo, P. F., Slowik, J. G., Worsnop, D. R., Davidovits, P., and Jimenez, J. L.: Particle morphology and density characterization by combined mobility and aerodynamic diameter measurements. Part 1: Theory, Aerosol Sci. Technol., 38, 1185–1205, doi:10.1080/027868290903907, 2004. 7245

DeMott, P. J., Sassen, K., Poellot, M. R., Baumgardner, D., Rogers, D. C., Brooks, S. D., Prenni, A. J., and Kreidenweis, S. M.: African dust aerosols as atmospheric ice nuclei, Geophys. Res. Lett., 30(4), 1732, doi:10.1029/2003gl017410, 2003. 7237

Drewnick, F., Hings, S. S., DeCarlo, P., Jayne, J. T., Gonin, M., Fuhrer, K., Weimer, S., Jimenez, J. L., Demerjian, K. L., Borrmann, S., and Worsnop, D. R.: A new time-of-flight aerosol mass spectrometer (TOF-AMS) - Instrument description and first field deployment, Aerosol Sci. Technol., 39, 637–658, doi:10.1080/02786820500182040, 2005. 7240

Drewnick, F., Hings, S. S., Alfarra, M. R., Prevot, A. S. H., and Borrmann, S.: Aerosol quantification with the Aerodyne Aerosol Mass Spectrometer: detection limits and ionizer background effects, Atmos. Meas. Tech., 2, 33–46, doi:10.5194/amt-2-33-2009, 2009. 7248

Falkovich, A. H., Ganor, E., Levin, Z., Formenti, P., and Rudich, Y.: Chemical and mineralogical analysis of individual mineral dust particles, J. Geophys. Res., 106, 18029–18036, doi:10.1029/2000jd900430, 2001. 7237

Forster, P., Ramaswamy, V., Artaxo, P., Berntsen, T., Betts, R., Fahey, D., Haywood, J., Lean, J., Lowe, D., Myhre, G., Nganga, J., Prinn, R., Raga, G., Schulz, M., and Van Dorland, R.: Changes in Atmospheric Constituents and in Radiative Forcing, in: Climate Change 2007: The Physical Science Basis. Contribution of Working Group I to the Fourth Assessment Report of the Intergovernmental Panel on Climate Change, edited by: Solomon, S., Qin, D., Manning, M., Chen, Z., Marquis, M., Averyt, K. B., Tignor, M., and Miller, H. L., Cambridge University Press, Cambridge, United Kingdom and New York, NY, USA, Cambridge, 2007. 7237

Gallavardin, S. J., Froyd, K. D., Lohmann, U., Möhler, O., Murphy, D. M., and Cziczo, D. J.: Single Particle Laser Mass Spectrometry Applied to Differential Ice Nucleation Experiments at the AIDA Chamber, Aerosol Sci. Technol., 42, 773–791, doi:10.1080/02786820802339538,

ACPD
11, 7235–7289, 2011

2008. 7238
Hartmann, S., Niedermeier, D., Voigtländer, J., Clauss, T., Shaw, R. A., Wex, H., Kiselev, A., and Stratmann, F.: Homogeneous and heterogeneous ice nucleation at LACIS: operating principle and theoretical studies, Atmos. Chem. Phys., 11, 1753–1767, doi:10.5194/acp-11-1753-2011, 2011. 7238, 7240, 7242
Hinz, K. P., Trimborn, A., Weingartner, E., Henning, S., Baltensperger, U., and Spengler, B.: Aerosol single particle composition at the Jungfraujoch, J. Aerosol Sci., 36, 123–145, doi:10.1016/j.jaerosci.2004.08.001, 2005. 7237
Huffman, J. A., Jayne, J. T., Drewnick, F., Aiken, A. C., Onasch, T., Worsnop, D. R., and Jimenez, J. L.: Design, modeling, optimization, and experimental tests of a particle beam width probe for the aerodyne aerosol mass spectrometer, Aerosol Sci. Technol., 39, 1143–1163, doi:10.1080/02786820500423782, 2005. 7244
IFA: GESTIS-material-database, available at: http://www.dguv.de/ifa/de/gestis/stoffdb/index.jsp, 2010. 7255, 7272
Jayne, J. T., Leard, D. C., Zhang, X. F., Davidovits, P., Smith, K. A., Kolb, C. E., and Worsnop, D. R.: Development of an aerosol mass spectrometer for size and composition analysis of submicron particles, Aerosol Sci. Technol., 33, 49–70, 2000. 7240, 7244, 7245
Kamphus, M., Ettner-Mahl, M., Klimach, T., Drewnick, F., Keller, L., Cziczo, D. J., Mertes, S., Borrmann, S., and Curtius, J.: Chemical composition of ambient aerosol, ice residues and cloud droplet residues in mixed-phase clouds: single particle analysis during the Cloud and Aerosol Characterization Experiment (CLACE 6), Atmos. Chem. Phys., 10, 8077–8095, doi:10.5194/acp-10-8077-2010, 2010. 7237
Kay, J. E., Baker, M., and Hegg, D.: Physical controls on orographic cirrus inhomogeneity, Atmos. Chem. Phys., 7, 3771–3781, doi:10.5194/acp-7-3771-2007, 2007. 7237
Klein, H., Nickovic, S., Haunold, W., Bundke, U., Nillius, B., Ebert, M., Weinbruch, S., Schuetz, L., Levin, Z., Barrie, L. A., and Bingemer, H.: Saharan dust and ice nuclei over Central Europe, Atmos. Chem. Phys., 10, 10211–10221, doi:10.5194/acp-10-10211-2010, 2010. 7258, 7261
Liu, P. S. K., Deng, R., Smith, K. A., Williams, L. R., Jayne, J. T., Canagaratna, M. R., Moore, K., Onasch, T. B., Worsnop, D. R., and Deshler, T.: Transmission efficiency of an aerodynamic focusing lens system: Comparison of model calculations and laboratory measurements for the Aerodyne Aerosol Mass Spectrometer, Aerosol Sci. Technol., 41, 721–733, doi:10.1080/02786820701422278, 2007. 7243

ACPD
11, 7235–7289, 2011

Lohmann, U. and Feichter, J.: Global indirect aerosol effects: a review, Atmos. Chem. Phys., 5, 715–737, doi:10.5194/acp-5-715-2005, 2005. 7237
Manson, J. E.: Calcium carbonate as an ice nucleus, J. Meteorol., 14, 85–86, 1957. 7258, 7261
Mason, B. J. and Maybank, J.: Ice-nucleating properties of some natural mineral dusts, Q. J. Roy. Meteorol. Soc., 84, 235–241, 1958. 7258, 7261
Matthew, B. M., Middlebrook, A. M., and Onasch, T. B.: Collection efficiencies in an Aerodyne Aerosol Mass Spectrometer as a function of particle phase for laboratory generated aerosols, Aerosol Sci. Technol., 42, 884–898, doi:10.1080/02786820802356797, 2008. 7244
Mertes, S., Verheggen, B., Walter, S., Connolly, P., Ebert, M., Schneider, J., Bower, K. N., Cozic, J., Weinbruch, S., Baltensperger, U., and Weingartner, E.: Counterflow virtual impactor based collection of small ice particles in mixed-phase clouds for the physico-chemical characterization of tropospheric ice nuclei : Sampler description and first case study, Aerosol Sci. Technol., 41, 848–864, doi:10.1080/02786820701501881, 2007. 7237
Möhler, O., Buttner, S., Linke, C., Schnaiter, M., Saathoff, H., Stetzer, O., Wagner, R., Krämer, M., Mangold, A., Ebert, V., and Schurath, U.: Effect of sulfuric acid coating on heterogeneous ice nucleation by soot aerosol particles, J. Geophys. Res.-Atmos., 110(12), D11210, doi:10.1029/2004jd005169, 2005. 7238
Möhler, O., Benz, S., Saathoff, H., Schnaiter, M., Wagner, R., Schneider, J., Walter, S., Ebert, V., and Wagner, S.: The effect of organic coating on the heterogeneous ice nucleation efficiency of mineral dust aerosols, Environ. Res. Lett., 3(8), 025007, doi:10.1088/1748-9326/3/2/025007, 2008. 7238, 7245
Niedermeier, D., Hartmann, S., Shaw, R. A., Covert, D., Mentel, T. F., Schneider, J., Poulain, L., Reitz, P., Spindler, C., Clauss, T., Kiselev, A., Hallbauer, E., Wex, H., Mildenberger, K., and Stratmann, F.: Heterogeneous freezing of droplets with immersed mineral dust particles – measurements and parameterization, Atmos. Chem. Phys., 10, 3601–3614, doi:10.5194/acp-10-3601-2010, 2010. 7238, 7239, 7256
Niedermeier, D., Hartmann, S., Clauss, T., Wex, H., Kiselev, A., Sullivan, R. C., DeMott, P. J., Petters, M. D., Reitz, P., Schneider, J., Mikhailov, E., Sierau, B., Stetzer, O., Reimann, B., Bundke, U., Shaw, R. A., Buchholz, A., Mentel, T. F., and Stratmann, F.: Experimental study of the role of chemical and physical surface processing on the IN ability of mineral dust particles, in preparation, 2011.
Nordmeyer, T. and Prather, K. A.: Real-time measurement capabilities using aerosol time-of-

ACPD
11, 7235–7289, 2011

flight mass-spectrometry, Anal. Chem., 66, 3540–3542, 1994. 7240
Petters, M. D. and Kreidenweis, S. M.: A single parameter representation of hygroscopic growth and cloud condensation nucleus activity, Atmos. Chem. Phys., 7, 1961–1971, doi:10.5194/acp-7-1961-2007, 2007. 7240
Petters, M. D. and Kreidenweis, S. M.: A single parameter representation of hygroscopic growth and cloud condensation nucleus activity – Part 2: Including solubility, Atmos. Chem. Phys., 8, 6273–6279, doi:10.5194/acp-8-6273-2008, 2008. 7241, 7256
Pruppacher, H. and Klett, J.: Microphysics of Clouds and Precipitation, p. 309, Kluwer Academic Publishers, The Netherlands, 2nd edn., 1997. 7242
Reitz P. and Schneider J.: Noise level determination by local cubic signal approximation: Calculation of Aerodyne Aerosol Mass Spectrometer Detection Limits, to be submitted to Atmos. Meas. Tech., 2011.
Richardson, M. S., DeMott, P. J., Kreidenweis, S. M., Cziczo, D. J., Dunlea, E. J., Jimenez, J. L., Thomson, D. S., Ashbaugh, L. L., Borys, R. D., Westphal, D. L., Casuccio, G. S., and Lersch, T. L.: Measurements of heterogeneous ice nuclei in the western United States in springtime and their relation to aerosol characteristics, J. Geophys. Res.-Atmos., 112(16), D02209, doi:10.1029/2006jd007500, 2007. 7237
Roberts, G. C. and Nenes, A.: A Continuous-Flow Streamwise Thermal-Gradient CCN Chamber for Atmospheric Measurements, Aerosol Sci. Technol., 39, 206–221, 2005. 7240
Roedel, W.: Physik unserer Umwelt: die Atmospäre, Springer-Verlag Berlin Heidelberg New York, 3rd edn., 2000. 7237
Rogers, D. C., DeMott, P. J., Kreidenweis, S. M., and Chen, Y.: A Continuous-Flow Diffusion Chamber for Airborne Measurements of Ice Nuclei, J. Atmos. Ocean. Tech., 18, 725–741, doi:10.1175/1520-0426(2001)018<0725:ACFDCF>2.0.CO;2, 2001. 7240
Schneider, J., Weimer, S., Drewnick, F., Borrmann, S., Helas, G., Gwaze, P., Schmid, O., Andreae, M. O., and Kirchner, U.: Mass spectrometric analysis and aerodynamic properties of various types of combustion-related aerosol particles, Int. J. Mass Spectrom., 258, 37–49, doi:10.1016/j.ijms.2006.07.008, 2006. 7250
Sitzmann, H.: Roempp Online – Version 3.5, available at: http://www.roempp.com/prod/ (last access: March 2011), 2004. 7272
Stratmann, F., Kiselev, A., Wurzler, S., Wendisch, M., Heintzenberg, J., Charlson, R. J., Diehl, K., Wex, H., and Schmidt, S.: Laboratory studies and numerical simulations of cloud droplet formation under realistic supersaturation conditions, J. Atmos. Ocean. Tech., 21, 876–887,

ACPD
11, 7235–7289, 2011

2004. 7238, 7240
Sullivan, R. C. and Prather, K. A.: Investigations of the Diurnal Cycle and Mixing State of Oxalic Acid in Individual Particles in Asian Aerosol Outflow, Environ. Sci. Technol., 41, 8062–8069, doi:10.1021/es071134g, 2007. 7237
Sullivan, R. C., Guazzotti, S. A., Sodeman, D. A., and Prather, K. A.: Direct observations of the atmospheric processing of Asian mineral dust, Atmos. Chem. Phys., 7, 1213–1236, doi:10.5194/acp-7-1213-2007, 2007. 7237
Sullivan, R. C., Moore, M. J. K., Petters, M. D., Kreidenweis, S. M., Roberts, G. C., and Prather, K. A.: Timescale for hygroscopic conversion of calcite mineral particles through heterogeneous reaction with nitric acid, Phys. Chem. Chem. Phys., 11, 7826–7837, 2009a. 7241
Sullivan, R. C., Moore, M. J. K., Petters, M. D., Kreidenweis, S. M., Roberts, G. C., and Prather, K. A.: Effect of chemical mixing state on the hygroscopicity and cloud nucleation properties of calcium mineral dust particles, Atmos. Chem. Phys., 9, 3303–3316, doi:10.5194/acp-9-3303-2009, 2009b. 7241, 7256
Sullivan, R. C., Miñambres, L., DeMott, P. J., Prenni, A. J., Carrico, C. M., Levin, E. J. T., and Kreidenweis, S. M.: Chemical processing does not always impair heterogeneous ice nucleation of mineral dust particles, Geophys. Res. Lett., 37, L24805, doi:10.1029/2010gl045540, 2010a. 7238
Sullivan, R. C., Petters, M. D., DeMott, P. J., Kreidenweis, S. M., Wex, H., Niedermeier, D., Hartmann, S., Clauss, T., Stratmann, F., Reitz, P., Schneider, J., and Sierau, B.: Irreversible loss of ice nucleation active sites in mineral dust particles caused by sulphuric acid condensation, Atmos. Chem. Phys., 10, 11471–11487, doi:10.5194/acp-10-11471-2010, 2010b. 7238, 7240, 7241, 7242, 7256, 7258, 7260, 7288
Svane, M., Hagström, M., and Pettersson, J. B. C.: Chemical analysis of individual alkali-containing aerosol particles: Design and performance of a surface ionization particle beam mass spectrometer, Aerosol Sci. Technol., 38, 655–663, doi:10.1080/02786820490485944, 2004. 7249
Svane, M., Hagström, M., and Pettersson, J. B. C.: Online measurements of individual alkali-containing particles formed in biomass and coal combustion: Demonstration of an instrument based on surface ionization technique, Energy Fuels, 19, 411–417, doi:10.1021/ef049925g, 2005. 7249
Timko, M. T., Yu, Z. H., Kroll, J. H., Jayne, J. T., Worsnop, D. R., Miake-Lye, R. C., Onasch, T. B., Liscinsky, D., Kirchstetter, T. W., Destaillats, H., Holder, A. L., Smith, J. D., and Wilson, K. R.:

ACPD
11, 7235–7289, 2011

Sampling Artifacts from Conductive Silicone Tubing, Aerosol Sci. Technol., 43, 855–865, doi:10.1080/02786820902984811, 2009. 7250

Vali, G.: Atmospheric Ice Nucleation – A Review, Journal de Recherches Atmospheriques, 19, 105–115, 1985. 7258

Vlasenko, A., Sjögren, S., Weingartner, E., Gäggeler, H. W., and Ammann, M.: Generation of submicron Arizona test dust aerosol: Chemical and hygroscopic properties, Aerosol Sci. Technol., 39, 452–460, doi:10.1080/027868290959870, 2005. 7249, 7250, 7256, 7272

Wex, H., Hennig, T., Salma, I., Ocskay, R., Kiselev, A., Henning, S., Massling, A., Wiedensohler, A., and Stratmann, F.: Hygroscopic growth and measured and modeled critical super-saturations of an atmospheric HULIS sample, Geophys. Res. Lett., 34(5), L02818, doi:10.1029/2006gl028260, 2007. 7240

Wex, H., Clauss, T., Covert, D., Hallbauer, E., Hartmann, S., Kiselev, A., Mentel, T. F., Mildenberger, K., Niedermeier, D., Poulain, L., Reitz, P., Schneider, J., Shaw, R., Spindler, C., and Stratmann, F.: Classifying Coated and Uncoated Arizona Test Dust with respect to Hygroscopic Growth and Activation, in preparation, 2011.

Wiacek, A. and Peter, T.: On the availability of uncoated mineral dust ice nuclei in cold cloud regions, Geophys. Res. Lett., 36(5), L17801, doi:10.1029/2009gl039429, 2009. 7237

Yu, Y., Alexander, M. L., Perraud, V., Bruns, E. A., Johnson, S. N., Ezell, M. J., and Finlayson-Pitts, B. J.: Contamination from electrically conductive silicone tubing during aerosol chemical analysis, Atmos. Environ., 43, 2836–2839, doi:10.1016/j.atmosenv.2009.02.014, 2009. 7250

Zhao, D. F., Buchholz, A., Mentel, Th. F., Müller, K.-P., Borchardt, J., Kiendler-Scharr, A., Spindler, C., Tillmann, R., Trimborn, A., Zhu, T., and Wahner, A.: Novel method of generation of $Ca(HCO_3)_2$ and $CaCO_3$ aerosols and first determination of hygroscopic and cloud condensation nuclei activation properties, Atmos. Chem. Phys., 10, 8601–8616, doi:10.5194/acp-10-8601-2010, 2010. 7249

Zimmermann, F., Weinbruch, S., Schütz, L., Hofmann, H., Ebert, M., Kandler, K., and Worringen, A.: Ice nucleation properties of the most abundant mineral dust phases, J. Geophys. Res., 113, D23204, doi:10.1029/2008jd010655, 2008. 7258, 7261

ACPD

11, 7235–7289, 2011

Table 1. Transmission correction factors: The errors have been estimated by varying the mode diameter and the geometric width in the range of the fitting parameter uncertainties.

particle type	correction factor
BCR 300 nm	1.45 ± 0.08
BCR 400 nm	2.31 ± 0.20
ATD 300 nm	1.50 ± 0.041
ATD 400 nm	3.0 ± 0.21

ACPD
11, 7235–7289, 2011

Table 2. Correction factors for the FROST campaigns in order to correct for systematic errors arising from the CPC accuracy, the CPC dilution stage and the AMS calibration accuracy.

campaign	correction factor
FROST1	0.459 ± 0.016
FROST2	2.18 ± 0.32

ACPD
11, 7235–7289, 2011

Table 3. Relative ionisation efficiencies (RIE) for the species sulphate and ammonium for the FROST1 and FROST2 campaign.

campaign	sulphate	ammonium
FROST1	0.615 ± 0.011	4.739 ± 0.079
FROST2	0.694 ± 0.024	6.08 ± 0.13

ACPD
11, 7235–7289, 2011

Table 4. Compilation of the percentage of particles showing a clear sulphate signal in the ATOFMS spectra after passing the sulphuric acid coating section. The temperature indicated is the temperature of the sulphuric acid coating bath. TD indicates the use of the thermodenuder which, if applied, was set to 250 °C for all experiments. WB marks experiments with the water bath in use and NH_3 refers to experiments during which ammonia was added to the aerosol.

Experiment	45°C	70 °C	70 °C TD	70 °C WB NH_3	70°C WB NH_3 TD	85°C
Conservative threshold [%]	97	92	96	84	93	89
Less conservative threshold [%]	100	95	100	93	95	94

ACPD
11, 7235–7289, 2011

Table 5. ATD surface elemental composition from XPS as found by Vlasenko et al. (2005) and possible compounds formed with these substances. Mg is expected to be on the particle surface as it is found in the bulk material, but the XPS data was recorded with an Mg anticathode, masking the Mg of the sample. The list shown below is only a proposal for possible reaction products based on the availability of the respective material. We were not able to directly identify these compounds. The numbers in the two last columns indicate the decomposition temperature T_d in °C and the solubility S_{20} at 20 °C in g l^{-1} (IFA, 2010).

element	fraction at ATD surface [%]	possible compounds	T_d	S_{20}
Na	2	Na_2SO_4	890	170
		$NaHSO_4$	315	1080
Mg	–	$MgSO_4$	1124	300
Al	24	$Al_2(SO_4)_3$	770	364
		$AlNH_4(SO_4)_2$	190[1]	150
Si	63	no information	–	–
K	3	K_2SO_4	1069[1]	111.1
		$KHSO_4$	195	490
Fe	3	$Fe(II)SO_4$	400	256
		$Fe(III)_2(SO_4)_3$	480	4400
		$NH_4Fe(III)(SO_4)_2$	41[1,2]	1240[3]
Ca	5	$CaSO_4$	700	2

[1]Melting temperature, [2]source: AlfaAeser (2010), [3]source: Sitzmann (2004) at 25 °C.

ACPD
11, 7235–7289, 2011

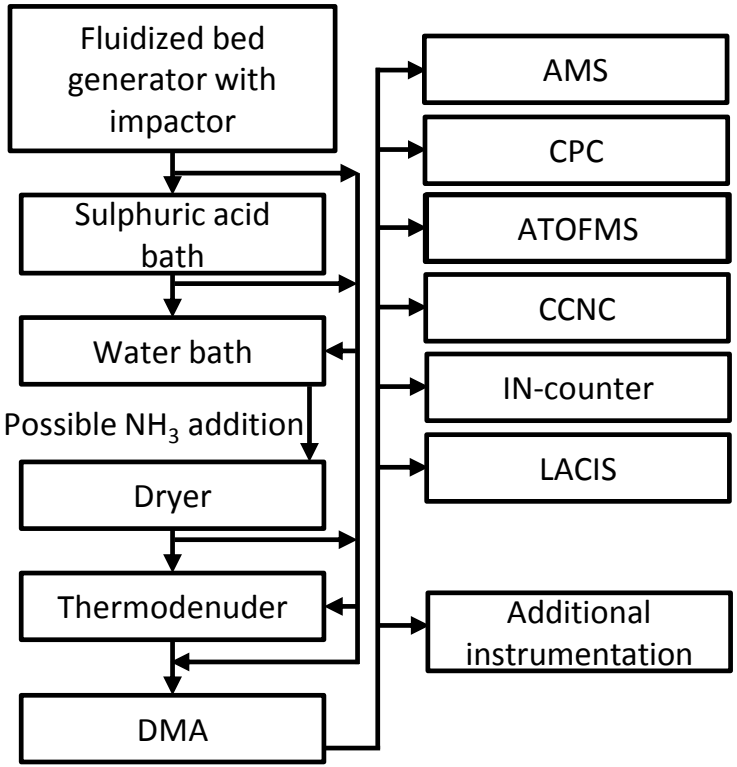

Fig. 1. Experimental set-up of the FROST campaigns. The sections between the Fluidized bed generator and the DMA can be bypassed.

ACPD
11, 7235–7289, 2011

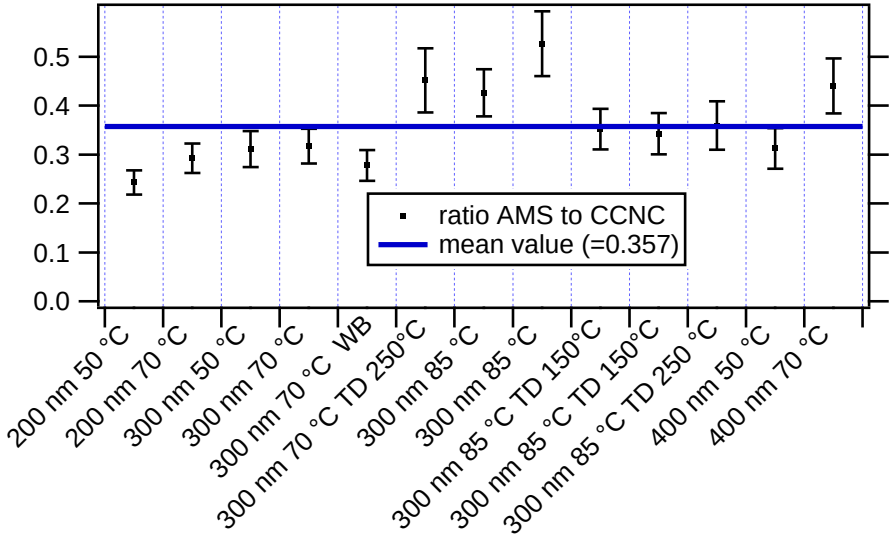

Fig. 2. Collection efficiency (CE) for all experiments using coated BCR particles.

ACPD
11, 7235–7289, 2011

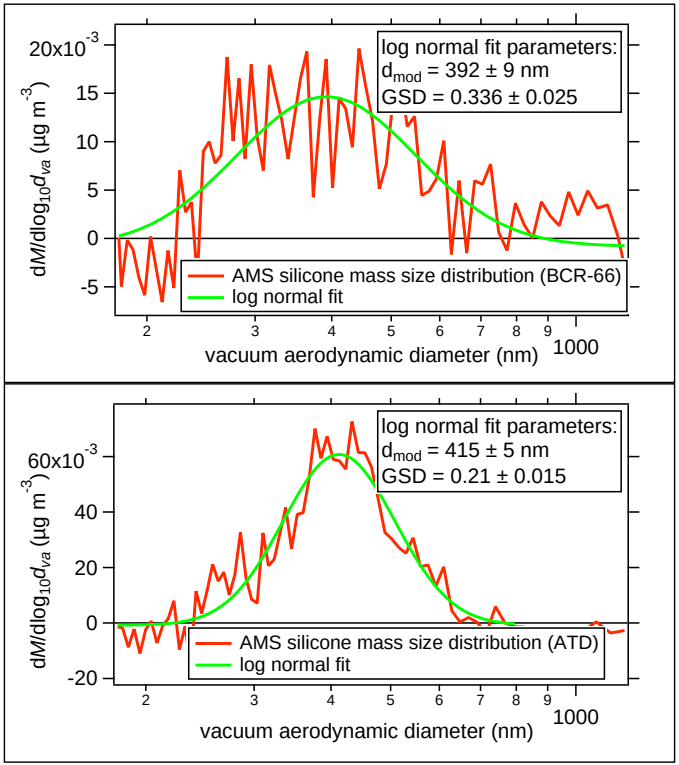

Fig. 3. Silicone size distributions for 200 nm mobility diameter particles with log normal fit. Upper graph: BCR, averaged over 1 h and 20 min; lower graph: ATD, averaged over 5 h and 39 min.

ACPD
11, 7235–7289, 2011

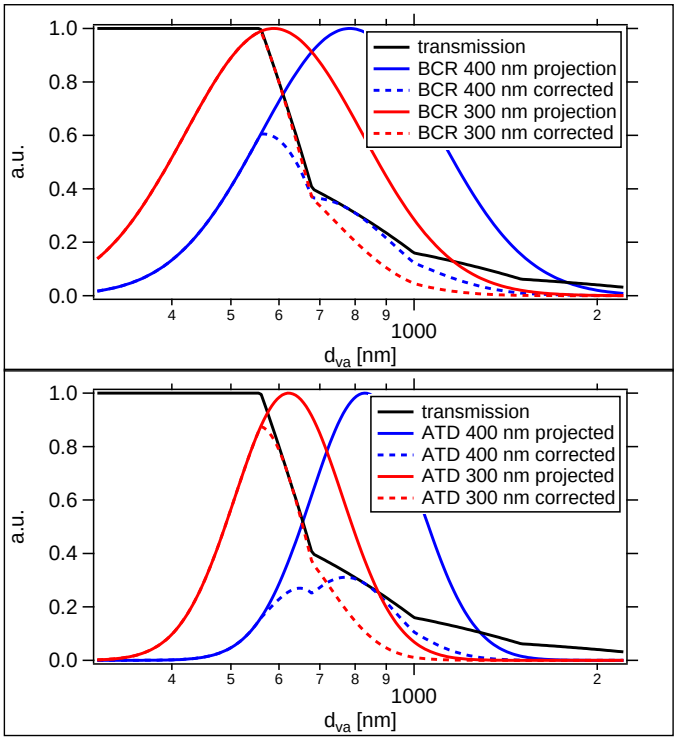

Fig. 4. Transmission correction for BCR and ATD particles. The figures show the projected transmission curves as calculated from the fits in Fig. 3 as well as the projected size distribution when the transmission of the aerodynamic lens is taken into account.

ACPD
11, 7235–7289, 2011

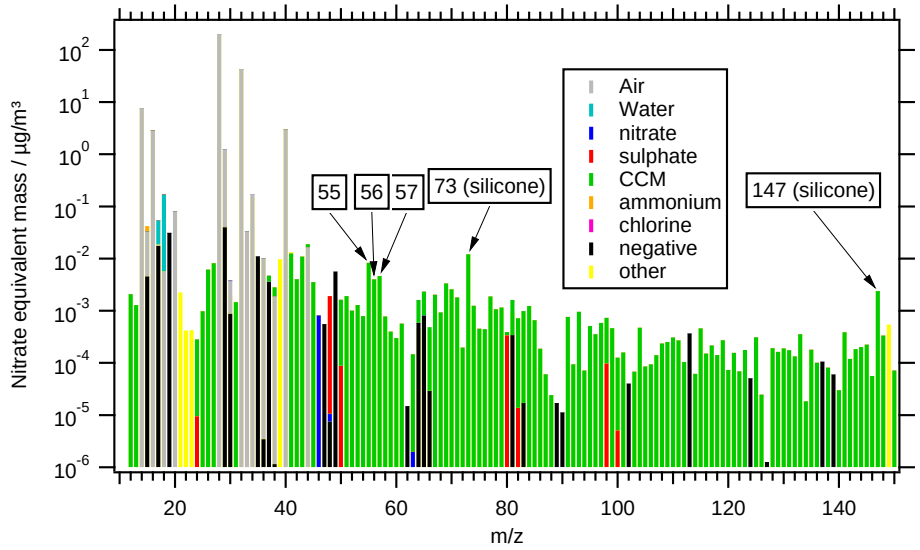

Fig. 5a. Average AMS mass spectrum for unprocessed ATD during the FROST1 campaign. Notable are the clear peaks that can be attributed to methyl silicone contaminant.

ACPD
11, 7235–7289, 2011

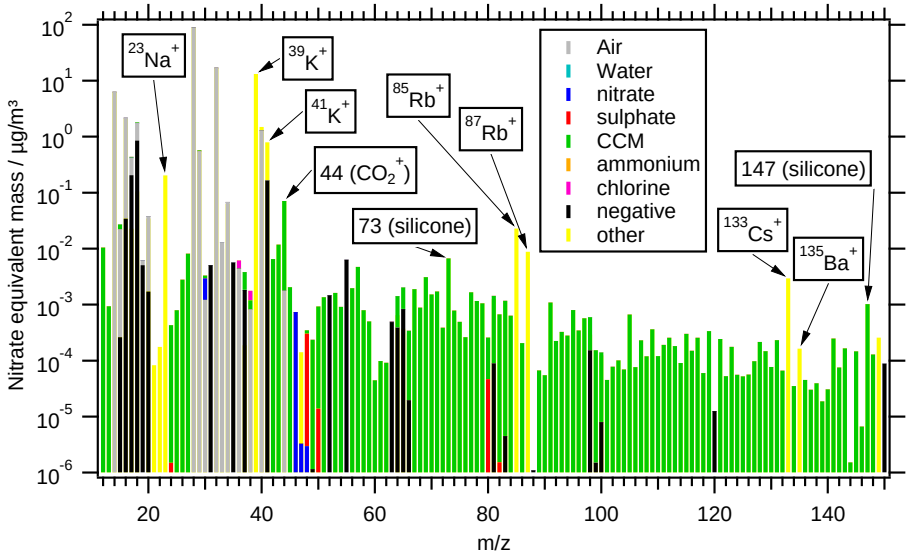

Fig. 5b. Average AMS mass spectrum for untreated ATD during the FROST2 campaign. Beside the silicone peaks already visible during FROST1, some new very distinct metal peaks show up in this spectrum, due to the elevated vaporiser temperature of 820 °C: $^{23}Na^+$, $^{39}K^+$, $^{41}K^+$, $^{85}Rb^+$, $^{87}Rb^+$, $^{133}Cs^+$ and $^{135}Ba^+$.

ACPD
11, 7235–7289, 2011

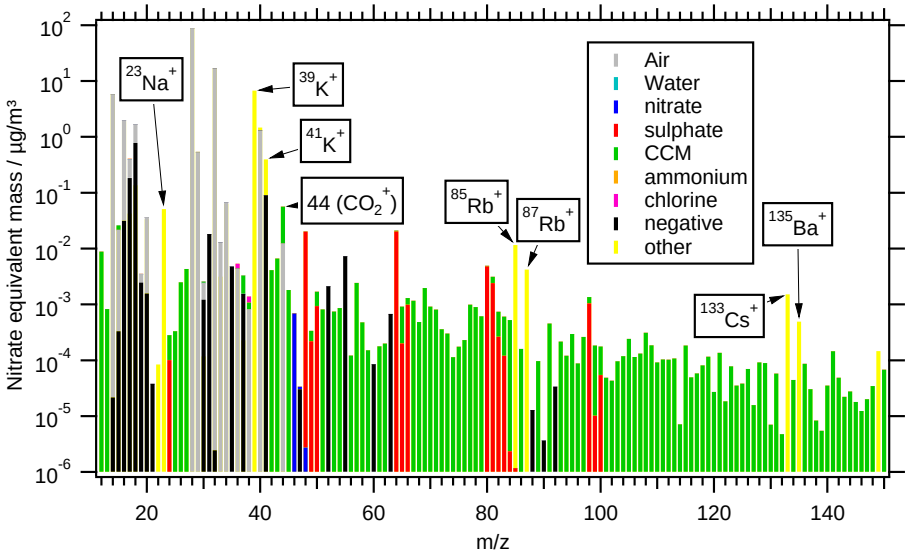

Fig. 5c. Average AMS mass spectrum of sulphuric acid processed ATD during the FROST2 campaign. The sulphuric acid bath temperature was 70 °C. Beside the sulphate peaks in red, the metal peaks that were already visible in the unprocessed 820 °C data remain visible. The silicone probably reacted with the sulphuric acid and is no longer visible.

ACPD
11, 7235–7289, 2011

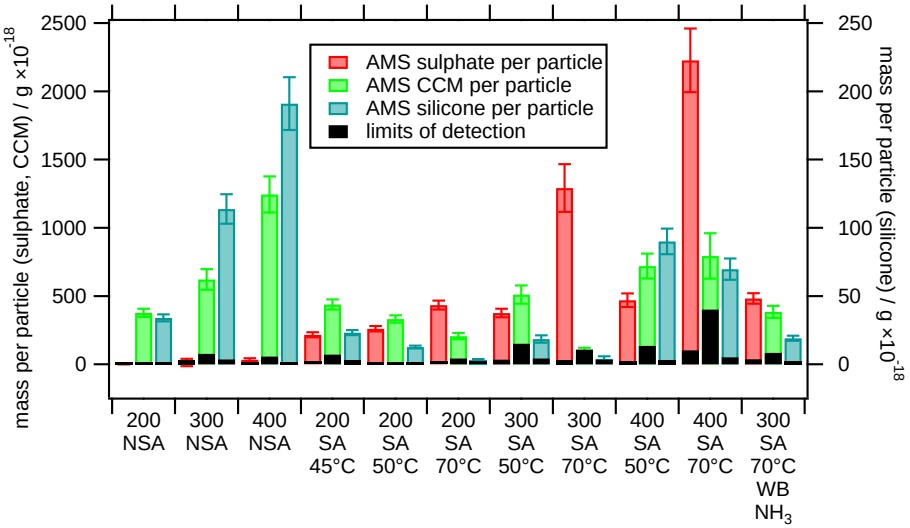

Fig. 6a. Summary of the mass per particle for the FROST1 campaign. First number of each category → particle diameter in nm, NSA → no sulphuric acid, SA → sulphuric acid and NH_3 → addition of ammonia. The temperature shown is the bath temperature for the respective coating substance. Note that the silicone axis is enhanced by a factor of 10 for clarity.

ACPD
11, 7235–7289, 2011

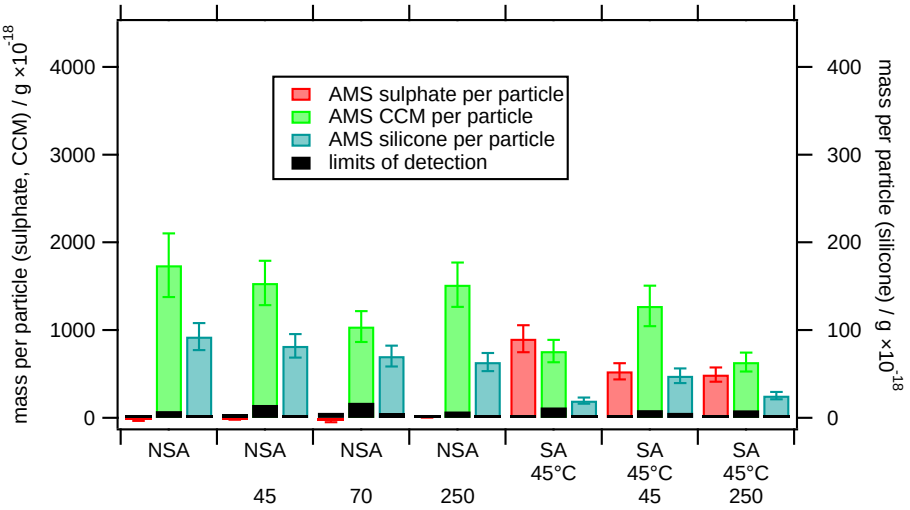

Fig. 6b. Summary of the mass per particle for the FROST2 campaigns' thinnest coating experiments. NSA → no sulphuric acid, SA → sulphuric acid, first number → sulphuric acid bath temperature and second number → thermodenuder temperature. Note that the silicone axis is enhanced by a factor of 10 for clarity. All particles had a mobility diameter of 300 nm.

ACPD
11, 7235–7289, 2011

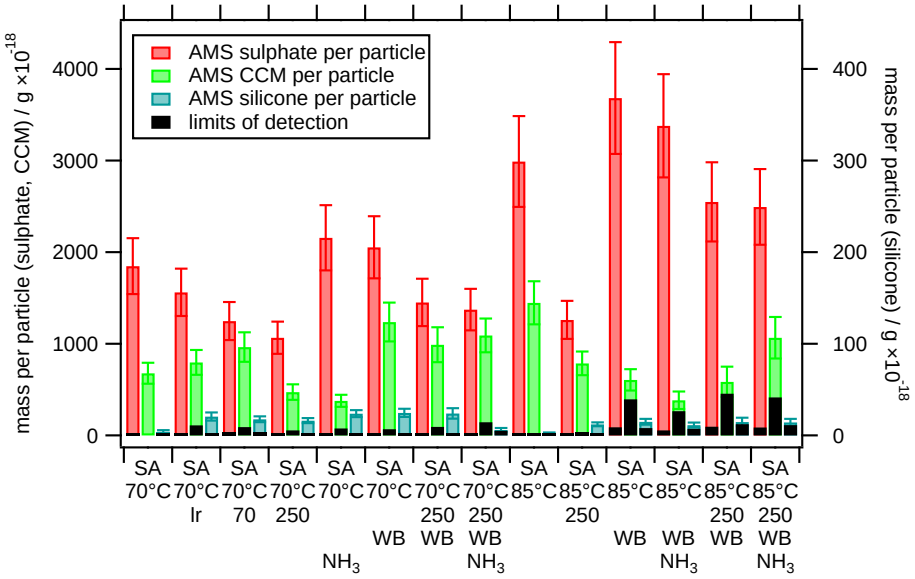

Fig. 6c. Summary of the mass per particle for the FROST2 campaign thicker coating experiments. lr → 10 l extra volume for longer residence time, SA → sulphuric acid, first number → sulphuric acid bath temperature, second number → thermodenuder temperature, WB → use of the water bath and NH_3 → addition of ammonia. Note that the silicone axis is enhanced by a factor of 10 for clarity. All particles had a mobility diameter of 300 nm.

ACPD
11, 7235–7289, 2011

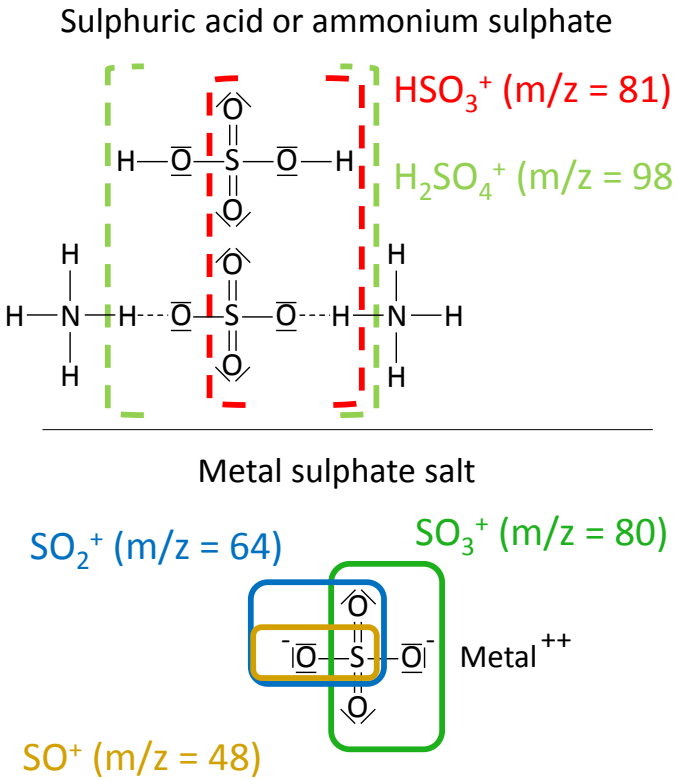

Fig. 7. Comparison between the possible fragments attributed to sulphate depending on the compound the sulphate is part of. For ammonium sulphate and sulphuric acid, hydrogen containing fragments are produced in the vaporisation and ionisation process while metal sulphate salts cannot produce such fragments.

ACPD
11, 7235–7289, 2011

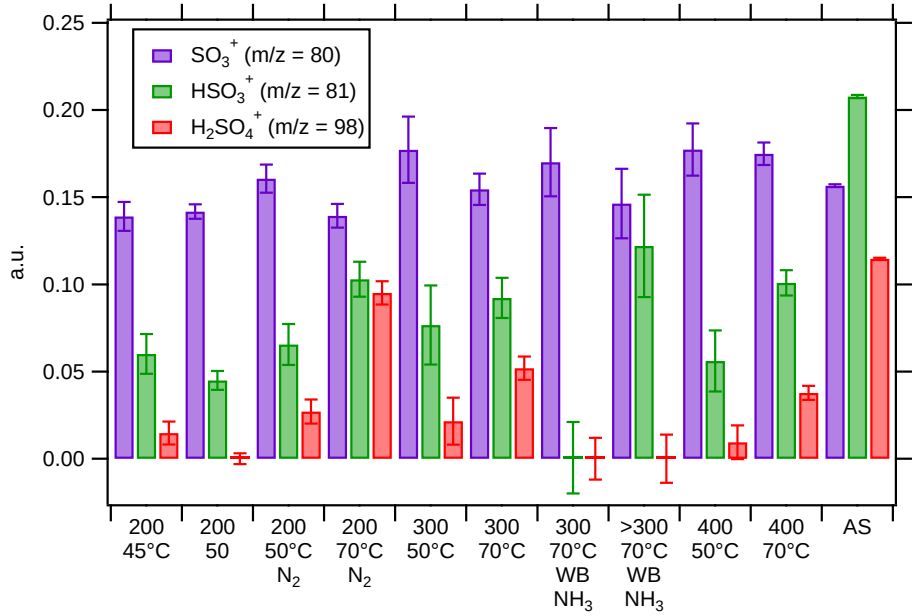

Fig. 8a. Intensity of the fragments $SO_3^+(m/z = 80)$, $HSO_3^+(m/z = 81)$ and $H_2SO_4^+(m/z = 98)$ normalised to the intensity of the fragment $SO_2^+(m/z = 64)$ for the FROST1 campaign. First number → particle mobility diameter, second number → sulphuric acid temperature, WB → use of the water bath, NH_3 → addition of ammonia and N_2 → use of nitrogen as carrier gas in the particle generation set-up before the DMA. AS is a pure ammonium sulphate measurement.

ACPD
11, 7235–7289, 2011

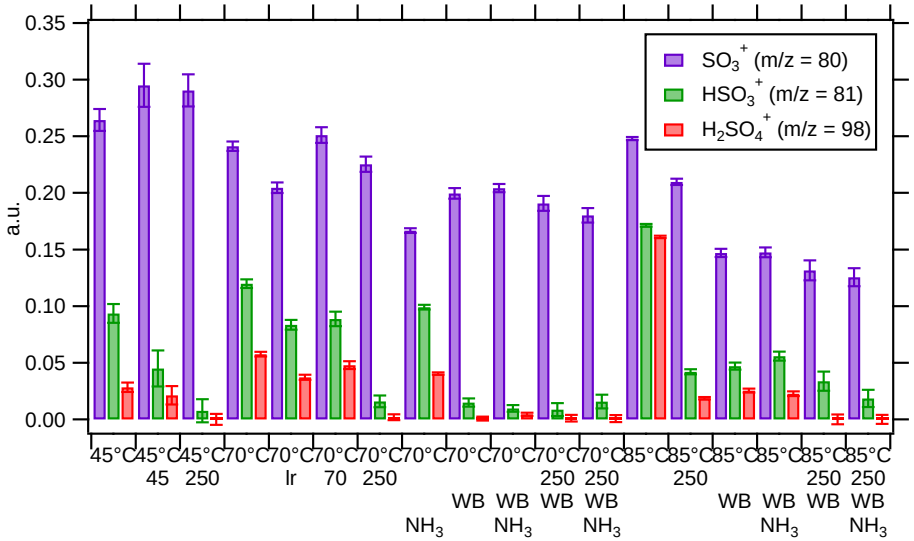

Fig. 8b. Intensity of the fragments SO_3^+(*m/z* = 80), HSO_3^+(*m/z* = 81) and $H_2SO_4^+$(*m/z* = 98) normalised to the intensity of the fragment SO_2^+(*m/z* = 64) for the FROST2 campaign. lr → 10 l extra volume for longer residence time, first number → sulphuric acid bath temperature, second number → thermodenuder temperature, WB → use of the water bath and NH_3 → addition of ammonia.

ACPD
11, 7235–7289, 2011

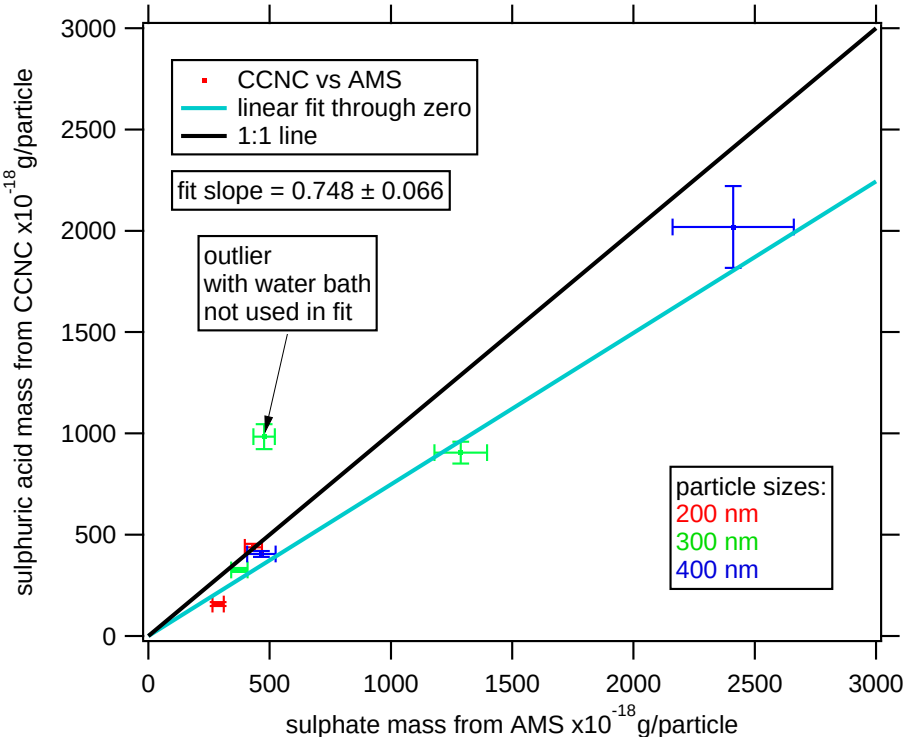

Fig. 9. Comparison of AMS sulphate mass per particle to CCNC soluble mass per particle for the FROST1 campaign. The outlier was recorded with the water bath in use.

ACPD
11, 7235–7289, 2011

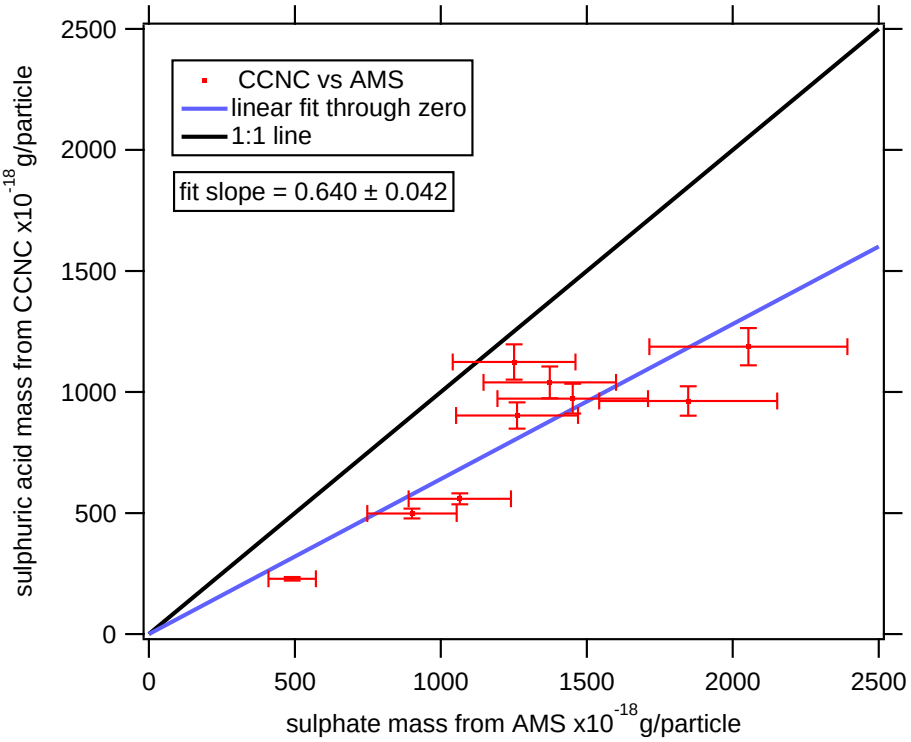

Fig. 10. Comparison of AMS sulphate mass per particle to CCNC soluble mass per particle for the FROST2 campaign.

ACPD
11, 7235–7289, 2011

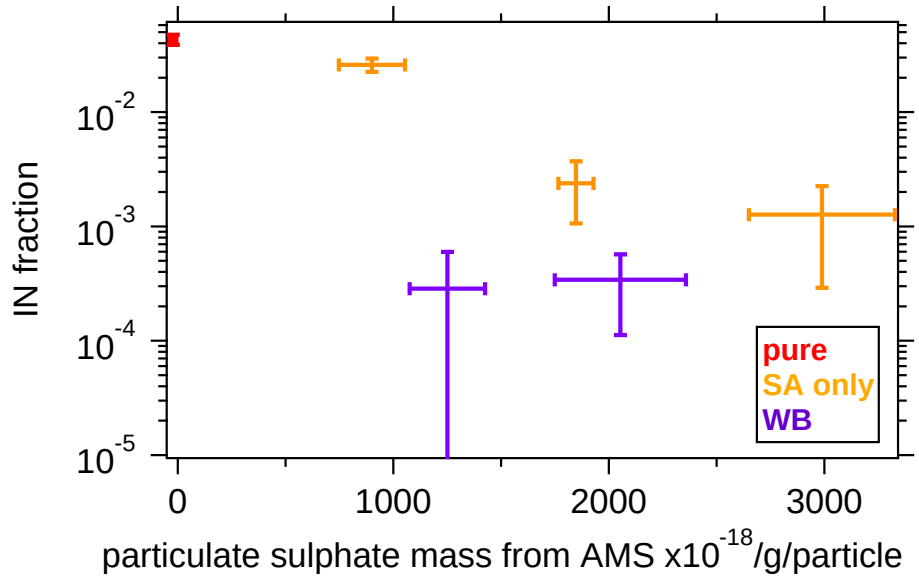

Fig. 11. Comparison of AMS sulphate mass per particle to CFDC ice nucleus counter at −30 °C in the immersion-freezing regime. This graph was modified after Sullivan et al. (2010b). Different coating temperatures are shown for the different particles classes. The particle class pure includes those experiments with no treatment and no sulphuric acid condensation. The particle class "SA only" includes particles which passed the sulphuric acid bath but no further processing was performed and WB indicates the use of the water bath. The IN-activity of the ATD is reduced if more sulphuric acid is condensed on the particle surface and the use of the water bath decreases the number of IN even further.

ACPD
11, 7235–7289, 2011

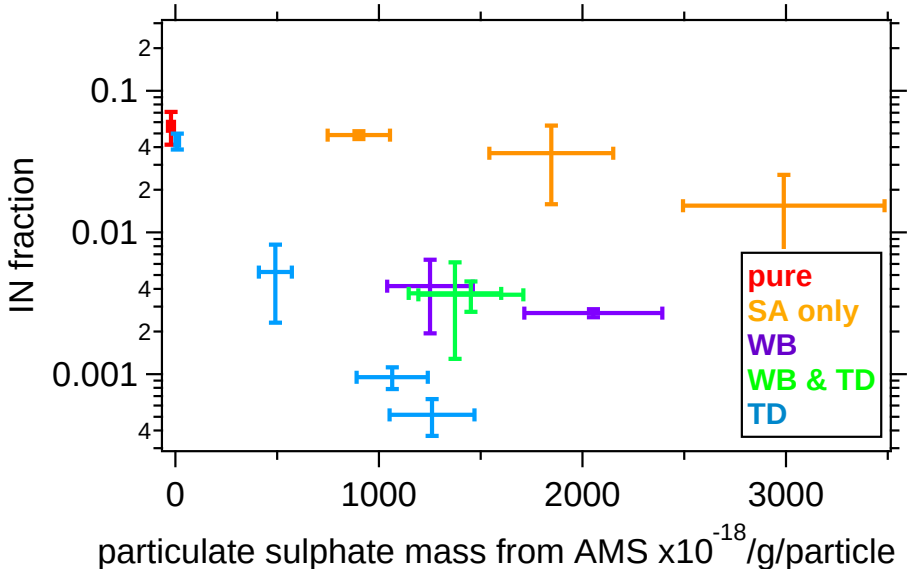

Fig. 12. Comparison of AMS sulphate mass per particle to the LACIS ice nucleus counts at −35 °C during FROST2. Different sulphuric acid bath temperatures are shown for every particle class. The particle class pure includes those experiments with no treatment and no sulphuric acid condensation. The particle class "SA only" includes particles which passed the sulphuric acid bath but no further processing was performed. WB indicates the use of the water bath and TD the use of the thermodenuder after the treatment except for the blue point on the upper left which passed the thermodenuder but was not coated.

ACPD
11, 7235–7289, 2011